Generation of two-temporal-mode photon states by vector four-wave mixing

Mckinstrie, C. J.; Christensen, Jesper Bjerge; Rottwitt, Karsten; Raymer, M. G.

Published in:
Optics Express

Link to article, DOI:
10.1364/OE.25.020877

Publication date:
2017

Document Version
Publisher's PDF, also known as Version of record

Research Article | Vol. 25, No. 17 | 21 Aug 2017 | OPTICS EXPRESS 20877
Optics EXPRESS

Generation of two-temporal-mode photon states by vector four-wave mixing

C. J. McKinstrie,[1,2,*] J. B. Christensen,[1] K. Rottwitt,[1] and M. G. Raymer[3]

[1]*Department of Photonics Engineering, Technical University of Denmark, 2800 Kongens Lyngby, Denmark*
[2]*Huawei Technologies, 400 Crossing Boulevard, Bridgewater, New Jersey 08807, USA*
[3]*Department of Physics, and Center for Optical, Molecular and Quantum Science, University of Oregon, Eugene, OR 97403, USA*

[*]*colin.mckinstrie@huawei.com*

Abstract: Photon pair states and multiple-photon squeezed states have many applications in quantum information science. In this paper, Green functions are derived for spontaneous four-wave mixing in the low- and high-gain regimes. Nondegenerate four-wave mixing in a strongly-birefringent medium generates signal and idler photons that are associated with only one pair of temporal (Schmidt) modes, for a wide range of pump powers and arbitrary pump shapes. The Schmidt coefficients (expected photon numbers) depend sensitively on the pump powers, and the Schmidt functions (shapes of the photon wavepackets) depend sensitively on the pump powers and shapes, which can be controlled.

OCIS codes: (190.4380) Nonlinear optics, four-wave mixing; (270.6570) Squeezed states.

References and links

1. M. A. Nielsen and I. L. Chuang, *Quantum Computation and Quantum Information* (Cambridge University, 2000).
2. N. Gisin, G. Ribordy, W. Tittel, and H. Zbinden, "Quantum cryptography," Rev. Mod. Phys. **74**, 145–195 (2002).
3. P. Kok, W. J. Munro, K. Nemoto, T. C. Ralph, J. P. Downing, and G. J. Milburn, "Linear optical quantum computing with photonic qubits," Rev. Mod. Phys. **79**, 135–174 (2007).
4. I. A. Walmsley, "Quantum optics: Science and technology in a new light," Science **348**, 525–530 (2015).
5. D. C. Burnham and D. L. Weinberg, "Observation of simultaneity in parametric production of optical photon pairs," Phys. Rev. Lett. **25**, 84–87 (1970).
6. R. W. Boyd, *Nonlinear Optics, 3rd Ed.* (Academic, 2008).
7. M. Fiorentino, P. L. Voss, J. E. Sharping, and P. Kumar, "All-fiber photon-pair source for quantum communications," IEEE Photon. Technol. Lett. **14**, 983–985 (2002).
8. M. E. Marhic, *Fiber Optical Parametric Amplifiers, Oscillators and Related Devices* (Cambridge University, 2007).
9. C. K. Hong, Z. Y. Ou, and L. Mandel, "Measurement of subpicosecond time intervals between two photons by interference," Phys. Rev. Lett. **59**, 2044–2046 (1987).
10. I. A. Walmsley and M. G. Raymer, "Toward quantum-information processing with photons," Science **307**, 1733–1734 (2005).
11. A. B. U'Ren, C. Silberhorn, K. Banaszek, I. A. Walmsley, R. Erdmann, W. P. Grice, and M. G. Raymer, "Generation of pure-state single-photon wavepackets by conditional preparation based on spontaneous parametric downconversion," Laser Phys. **15**, 146–161 (2005).
12. K. Garay-Palmett, H. J. McGuinness, O. Cohen, J. S. Lundeen, R. Rangel-Rojo, A. B. U'Ren, M. G. Raymer, C. J. McKinstrie, S. Radic, and I. A. Walmsley, "Photon pair-state preparation with tailored spectral properties by spontaneous four-wave mixing in photonic-crystal fiber," Opt. Express **15**, 14870–14886 (2007).
13. P. J. Mosley, J. S. Lundeen, B. J. Smith, P. Wasylczyk, A. B. U'Ren, C. Silberhorn, and I. A. Walmsley, "Heralded generation of ultrafast single photons in pure quantum states," Phys. Rev. Lett. **100**, 133601 (2008).
14. M. Halder, J. Fulconis, B. Cemlyn, A. Clark, C. Xiong, W. J. Wadsworth, and J. G. Rarity, "Nonclassical 2-photon interference with separate intrinsically narrowband fibre sources," Opt. Express **17**, 4670–4676 (2009).
15. A. I. Lvovsky, "Squeezed light," in *Photonics: Scientific Foundations, Technology and Applications, Volume 1*, edited by D. Andrews (Wiley, 2015), pp. 121–164.
16. M. Chekhova, G. Leuchs, and M. Zukowski, "Bright squeezed vacuum: Entanglement of macroscopic light beams," Opt. Commun. **337**, 27–43 (2015).
17. O. Aytur and P. Kumar, "Pulsed twin beams of light," Phys. Rev. Lett. **65**, 1551–1554 (1990).
18. J. E. Sharping, M. Fiorentino, and P. Kumar, "Observation of twin-beam-type quantum correlation in optical fiber," Opt. Lett. **26**, 367–369 (2001).

#295794 https://doi.org/10.1364/OE.25.020877
Journal © 2017 Received 10 May 2017; revised 9 Aug 2017; accepted 11 Aug 2017; published 18 Aug 2017

Optics EXPRESS

19. Z. Y. Ou, S. F. Pereira, H. J. Kimble, and K. C. Peng, "Realization of the Einstein-Podolsky-Rosen paradox for continuous variables," Phys. Rev. Lett. **68**, 3663–3666 (1992).
20. M. D. Reid, P. D. Drummond, W. P. Bowen, E. G. Cavalcanti, P. K. Lam, H. A. Bachor, U. L. Andersen, and G. Leuchs, "The Einstein-Podolsky-Rosen paradox: From concepts to applications," Rev. Mod. Phys. **81**, 1727–1751 (2009).
21. M. Cooper, L. J. Wright, C. Söller, and B. J. Smith, "Experimental generation of multi-photon Fock states," Opt. Express **21**, 5311–5317 (2013).
22. A. Ourjoumtsev, H. Jeong, R. Tualle-Brouri, and P. Grangier, "Generation of optical Schrödinger cats from photon number states," Nature **448**, 784–786 (2007).
23. S. L. Braunstein and P. van Loock, "Quantum information with continuous variables," Rev. Mod. Phys. **77**, 513–577 (2005).
24. U. L. Andersen, G. Leuchs and C. Silberhorn, "Continuous-variable quantum information processing," Laser Photon. Rev. **4**, 337–354 (2010).
25. D. Gottesman and J. Preskill, "Secure quantum key distribution using squeezed states," Phys. Rev. A **63**, 022309 (2001).
26. A. C. Funk and M. G. Raymer, "Quantum key distribution using non-classical photon number correlations in macroscopic light pulses," Phys. Rev. A **65**, 042307 (2002).
27. A. Furusawa, J. L. Sorensen, S. L. Braunstein, C. A. Fuchs, H. J. Kimble, and E. S. Polzik, "Unconditional quantum teleportation," Science **282**, 706–709 (1998).
28. N. Lee, H. Benichi, Y. Takeno, S. Takeda, J. Webb, E. Huntington, and A. Furusawa, "Teleportation of nonclassical wave packets of light," Science **332**, 330–332 (2011).
29. V. Giovannetti, S. Lloyd, and L. Maccone, "Quantum-enhanced measurements: Beating the standard quantum limit," Science **306**, 1330–1336 (2004).
30. J. P. Dowling and K. P. Seshadreesan, "Quantum Optical Technologies for Metrology, Sensing, and Imaging," J. Lightwave Technol. **33**, 2359–2370 (2015).
31. M. Xiao, L. A. Wu, and H. J. Kimble, "Precision measurement beyond the shot-noise limit," Phys. Rev. Lett. **59**, 278–281 (1987).
32. G. Y. Xiang, H. F. Hofmann, and G. J. Pryde, "Optimal Multi-Photon Phase Sensing with a Single Interference Fringe," Sci. Rep. **3** 2684 (2013).
33. C. M. Caves, "Quantum-mechanical noise in an interferometer," Phys. Rev. D **23**, 1693–1708 (1981).
34. R. Schnabel, N. Mavalvala, D. E. McClelland, and P. K. Lam, "Quantum metrology for gravitational wave astronomy," Nat. Commun. **1**, 121 (2010).
35. B. Yurke, S. L. McCall, and J. R. Klauder, "SU(2) and SU(1,1) interferometers," Phys. Rev. A **33**, 4033–4054 (1986).
36. F. Hudelist, J. Kong, C. Liu, J. Jing, Z. Y. Ou, and W. Zhang, "Quantum metrology with parametric amplifier-based photon correlation interferometers," Nat. Commun. **5**, 3049 (2014).
37. S. L. Braunstein, "Squeezing as an irreducible resource," Phys. Rev. A **71**, 055801 (2005).
38. W. Wasilewski, A. I. Lvovsky, K. Banaszek, and C. Radzewicz, "Pulsed squeezed light: Simultaneous squeezing of multiple modes," Phys. Rev. A **73**, 063819 (2006).
39. C. J. McKinstrie and M. Karlsson, "Schmidt decompositions of parametric processes I: Basic theory and simple examples," Opt. Express **21**, 1374–1394 (2013).
40. G. Ferrini, I. Fsaifes, T. Labidi, F. Goldfarb, N. Treps and F. Bretenaker, "Symplectic approach to the amplification process in a nonlinear fiber: role of signal-idler correlations and application to loss management," J. Opt. Soc. Am. B **31**, 1627–1641 (2014).
41. R. Loudon, *The Quantum Theory of Light, 3rd Ed.* (Oxford University, 2000).
42. C. C. Gerry and P. L. Knight, *Introductory Quantum Optics* (Cambridge University, 2005). Two-mode squeezed vacuum states are discussed in Sec. 7.7.
43. B. Fang, O. Cohen, J. B. Moreno, and V. O. Lorenz, "State engineering of photon pairs produced through dual-pump spontaneous four-wave mixing," Opt. Express **21**, 2707–2717 (2013).
44. J. B. Christensen, C. J. McKinstrie, and K. Rottwitt, "Temporally uncorrelated photon-pair generation by dual-pump four-wave mixing," Phys. Rev. A **94**, 013819 (2016).
45. C. J. McKinstrie and G. G. Luther, "The modulational instability of colinear waves," Phys. Scripta **30**, 31–40 (1990).
46. J. E. Rothenberg, "Modulational instability for normal dispersion," Phys. Rev. A **42**, 682–685 (1990).
47. P. D. Drummond, T. A. B. Kennedy, J. M. Dudley, R. Leonhardt and J. D. Harvey, "Cross-phase modulational instability in high-birefringence fibers," Opt. Commun. **78**, 137–142 (1990).
48. D. Amans, E. Brainis, M. Haelterman, P. Emplit, and S. Massar, "Vector modulation instability induced by vacuum fluctuations in highly birefringent fibers in the anomalous-dispersion regime," Opt. Lett. **30**, 1051–1053 (2005).
49. M. G. Raymer, "Quantum state entanglement and readout of collective atomic-ensemble modes and optical wave packets by stimulated Raman scattering," J. Mod. Opt. **51**, 1739–1759 (2004).
50. L. Mejling, C. J. McKinstrie, M. G. Raymer, and K. Rottwitt, "Quantum frequency translation by four-wave mixing in a fiber: low-conversion regime," Opt. Express **20**, 8367–8396 (2012).
51. C. J. McKinstrie, L. Mejling, M. G. Raymer, and K. Rottwitt, "Quantum-state preserving optical frequency conversion and pulse reshaping by four-wave mixing," Phys. Rev. A **85**, 053829 (2012).
52. B. Brecht, D. V. Reddy, C. Silberhorn, and M. G. Raymer, "Photon temporal modes: A complete framework for

Optics EXPRESS

quantum information science," Phys. Rev. X **5**, 041017 (2015).
53. M. G. Raymer and J. Mostowski, "Stimulated Raman scattering: Unified treatment of spontaneous initiation and spatial propagation," Phys. Rev. A **24**, 1980–1993 (1981).
54. R. E. Giacone, C. J. McKinstrie, and R. Betti, "Angular dependence of stimulated Brillouin scattering in homogeneous plasma," Phys. Plasmas **2**, 4596–4605 (1995).
55. M. G. Raymer, K. Rzazewski, and J. Mostowski, "Pulse-energy statistics in stimulated Raman scattering," Opt. Lett. **7**, 71–73 (1982).
56. D. L. Bobroff, "Coupled-modes analysis of the photon-photon parametric backward-wave oscillator," J. Appl. Phys. **36**, 1760–1769 (1965).
57. M. G. Raymer, Z. W. Li, and I. A. Walmsley, "Temporal quantum fluctuations in stimulated Raman scattering: Coherent-modes description," Phys. Rev. Lett. **63**, 1586–1589 (1989).
58. N. Liu, Y. Liu, X. Guo, L. Yang, X. Li, and Z. Y. Ou, "Approaching single temporal mode operation in twin beams generated by pulse pumped high gain spontaneous four wave mixing," Opt. Express **24**, 1096–1108 (2016).
59. L. Mejling, D. S. Cargill, C. J. McKinstrie, K. Rottwitt, and R. O. Moore, "Effects of nonlinear phase modulation on Bragg scattering in the low-conversion regime," Opt. Express **20**, 27454–27475 (2012).
60. B. Bell, A. McMillan, W. McCutcheon, and J. Rarity, "On the effects of self- and cross-phase modulation on photon purity for four-wave mixing photon-pair sources," Phys. Rev. A. **92**, 053849 (2015).
61. G. F. Sinclair and M. G. Thompson, "Effect of self- and cross-phase modulation on photon pairs generated by spontaneous four-wave mixing in integrated optical waveguides," Phys. Rev. A **94**, 063855 (2016).
62. C. J. McKinstrie, J. B. Christensen, K. Rottwitt, and M. G. Raymer, "Single-temporal-mode photon generation beyond the low-power regime," Quantum Information and Measurement conference, Paris, France, 5–7 April 2017, paper QW3C.6. In the simulations, $\beta_1 = 10$ ps/cm, $\beta_2 = 0.2$ ps^2/cm and $l = 1.0$ cm.

1. Introduction

Photons are a key resource for quantum information science [1–4]. Pairs of signal and idler photons can be generated by spontaneous three-wave mixing (TWM) in a second-order nonlinear medium [5], which is driven by one pump wave [6], and spontaneous four-wave mixing (FWM) in a third-order nonlinear medium [7], which can be driven by one or two pump wave(s) [8]. Detecting the idler photons heralds the existence of the associated signal photons, which subsequently can be used in quantum information protocols. Many of these protocols are similar to Hong-Ou-Mandel (HOM) interference [9], which requires the photons to be in pure indistinguishable states [10].

For many wave-mixing processes, the frequency bandwidths associated with wavenumber matching are much broader than the pump bandwidths, so the emitted photons occupy many spectral (temporal) modes. Heralding multiple-mode idler photons by direct detection leaves the associated signal photons in mixed states, which are not suitable for interference. One can reduce the numbers of modes and increase the heralded signal purities by using narrow-bandwidth frequency filters, but doing so also reduces the emission probabilities significantly. Alternatively, one can design sources based on wave mixing in such a way that the emitted photons occupy only single pairs of temporal modes [11–14]. Such designs typically involve relations between the inverse group speeds of the pump(s), signal and idler, the pump bandwidth(s) and the medium length. Sources driven by low-power pumps emit photon pairs with low probabilities. One can increase the emission probabilities by increasing the pump power(s), subject to the fundamental constraints that the emitted photons continue to occupy single pairs of modes, and the relative probabilities of quadruplet and pair states remain low.

Sources driven by high-power pumps produce two-continuous-mode squeezed states with multiple-photon wavepackets [15, 16]. Such states are entangled in the number-state basis (the numbers of signal and idler photons are strongly correlated [17, 18]) and the quadrature basis (if the signal and idler position quadratures are correlated, then their momentum quadratures are anti-correlated). Squeezed states enable fundamental tests of quantum mechanics [19, 20], and can be used to make other interesting states, such as multiple-photon Fock states [21] and Schrödinger cat states [22]. They also enable many aspects of continuous-variable (CV) quantum information [23, 24], including quantum key-distribution [25, 26], quantum teleportation [27, 28] and quantum-enhanced metrology [29, 30], which utilizes phase squeezing [31, 32], number squeezing [33, 34] and number-difference squeezing [35, 36] to reduce measurement errors below

Optics EXPRESS

the shot-noise limit. To work well, these applications also require the signal and idler photons to occupy single pairs of temporal modes (wavepackets with specific shapes). In this paper, we show theoretically that vector FWM in a strongly-birefringent medium (SBM) can satisfy this requirement.

In Sec. 2, we review the mathematics and physics of two-continuous-mode squeezing, in both the Heisenberg picture (HP) and the Schrödinger picture (SP). We also describe a temporal-mode (Schmidt) decomposition [37–40], which allows this two-continuous-mode process to be reformulated as a set of independent, two-discrete-mode processes, the properties of which are known [41,42]. Although it is easy to establish the general properties of Schmidt decompositions, it is often difficult to make specific decompositions. In Sec. 3, we review the generation of photons by nondegenerate FWM in the low-gain regime, and show that processes in which the first pump copropagates with the signal and the second pump copropagates with the idler enable the generation of photons in single pairs of Schmidt modes [43,44]. One such process is vector FWM in a SBM [45–48]. In Sec. 4, we model the generation of multiple-photon wavepackets by this process, in the high-gain regime. We determine the Green functions analytically and decompose them numerically. The results show that single-mode operation is possible for a wide variety of pump powers and arbitrary pump shapes. In Sec. 5, we discuss the effects of nonlinear phase modulation (NPM) briefly. For moderate pump powers, NPM chirps the photon wavepackets, but does not hinder the generation of single Schmidt-mode pairs. Finally, in Sec. 6 we summarize the main results of the paper.

2. Four-wave mixing

In nondegenerate FWM [8], two strong pump waves (p and q) drive weak signal (s) and idler (r) waves ($\pi_p + \pi_q \rightarrow \pi_r + \pi_s$, where π_j represents a photon with carrier frequency ω_j). In stimulated FWM, the signal and idler (sideband) growth is seeded by an input signal pulse, whereas in spontaneous FWM, the sideband growth is seeded by vacuum fluctuations (which one can think of as virtual pulses). In classical mechanics, the signal and idler waves (modes) evolve according to the coupled-mode equations (CMEs)

$$(\partial_z + \beta_r \partial_t) A_r(t,z) = i\gamma_{pq}(t,z) A_s^*(t,z), \tag{1}$$

$$(\partial_z + \beta_s \partial_t) A_s(t,z) = i\gamma_{pq}(t,z) A_r^*(t,z), \tag{2}$$

where A_j is a mode amplitude and β_j is a group slowness (inverse group speed). The pump function $\gamma_{pq}(t,z) = \gamma A_p(t-\beta_p z) A_q(t-\beta_q z)$, where $\gamma = \gamma_K \epsilon (E_p E_q)^{1/2}$ is proportional to the Kerr nonlinearity coefficient and the square roots of the pump energies. For parallel (perpendicular) pumps, $\epsilon = 2$ (2/3). Pump depletion is neglected, so the pump amplitudes A_p and A_q are specified functions, which are normalized in such a way that $\int dt |A_j(t)|^2 = 1$. These CMEs describe pulses that interact (unstably) as they convect through the medium. In the Heisenberg picture (HP) of quantum mechanics, one replaces the signal and idler amplitudes by the operators a_s and a_r, which satisfy the continuous commutation relations $[a_j(t,z), a_k(t',z)] = 0$ and $[a_j(t,z), a_k^\dagger(t',z)] = \delta_{jk}\delta(t-t')$, where δ_{jk} is the Kronecker delta and $\delta(t)$ is the Dirac delta function [41,42]. (The strong pumps are still treated classically.) The simple relation between the classical and quantum CMEs is not accidental: For systems with Hamiltonians that depend quadratically on the mode amplitudes (operators), the Heisenberg equations for the mode operators are identical to the Hamilton equations for the mode amplitudes.

Because the CMEs are linear in the mode operators, their solutions can be written in the input–output (IO) forms

$$b_r(t) = \int dt' [\mu_{rr}(t,t') a_r(t') + \nu_{rs}(t,t') a_s^\dagger(t')], \tag{3}$$

$$b_s(t) = \int dt' [\mu_{ss}(t,t') a_s(t') + \nu_{sr}(t,t') a_r^\dagger(t')], \tag{4}$$

Optics EXPRESS

where a_j and b_j denote input ($z = 0$) and output ($z = l$) operators, respectively. In these solutions, the transfer (Green) functions $\mu_{rr}(t,t')$ and $\nu_{rs}(t,t')$ describe the effects on the output idler of impulses applied to the input idler and signal, respectively. These impulses could represent short input pulses or vacuum fluctuations. A similar statement applies to $\mu_{ss}(t,t')$ and $\nu_{sr}(t,t')$. Henceforth, we will state results mainly for the idler, because the corresponding signal results can be deduced by interchanging subscripts ($r \leftrightarrow s$).

Because quantum evolution is unitary, the output mode operators must satisfy the same commutation relations as the input operators. It follows from two of these relations that

$$\int dt'[\mu_{rr}(t_1,t')\mu^*_{rr}(t_2,t') - \nu_{rs}(t_1,t')\nu^*_{rs}(t_2,t')] = \delta(t_1 - t_2), \quad (5)$$

$$\int dt'[\mu_{rr}(t_1,t')\nu_{sr}(t_2,t') - \nu_{rs}(t_1,t')\mu_{ss}(t_2,t')] = 0. \quad (6)$$

Every complex kernel $\mu(t,t')$ has the Schmidt decomposition $\sum_n v_n(t)\mu_n u^*_n(t')$, where μ_n is a Schmidt coefficient, and $u_n(t')$ and $v_n(t)$ are input and output Schmidt functions, respectively. The coefficients are real and non-negative, and the input (output) functions are orthonormal. Constraints (5) and (6) cause the idler Green functions to have the related decompositions

$$\mu_{rr}(t,t') = \sum_n v_{rn}(t)\mu_n u^*_{rn}(t'), \quad \nu_{rs}(t,t') = \sum_n v_{rn}(t)\nu_n u_{sn}(t'), \quad (7)$$

where n is the Schmidt-mode index and $\mu_n^2 - \nu_n^2 = 1$ [37–40]. The signal Green functions have similar decompositions (which involve the same coefficients). In stimulated FWM, the input functions are the natural shapes of the input pulses, the output functions are the shapes of the associated output pulses and the squared coefficients μ_n^2 are the associated energy gains. In spontaneous FWM, the input functions comprise a natural basis with which to describe the vacuum fluctuations, the output functions are the shapes of the associated output wavepackets and the squared coefficients ν_n^2 are the photon emission probabilities. The squared output functions describe the relative probilities that photons leave the medium at specific output times. One can interpret the squared input functions as the relative probabilities that photon generation was initiated (seeded) by virtual photons that entered the medium at specific input times. The Schmidt coefficients and functions depend on the physical parameters of the system, such as the pump powers, durations and slownesses, the sideband slownesses and the medium length.

If the sideband operators are decomposed in terms of Schmidt modes [$a_{rn} = \int dt' u^*_{rn}(t')a_r(t')$ and $b_{rn} = \int dt' v^*_{rn}(t')b_r(t')$], the Schmidt-mode operators satisfy the discrete commutation relations $[a_{rm}, a_{rn}] = 0$ and $[a_{rm}, a^\dagger_{rn}] = \delta_{mn}$. Each pair of operators undergoes the two-mode stretching (squeezing) transformation [49]

$$b_{rn} = \mu_n a_{rn} + \nu_n a^\dagger_{sn}, \quad b_{sn} = \mu_n a_{sn} + \nu_n a^\dagger_{rn}, \quad (8)$$

the properties of which are known [41, 42]. In particular, if the input is a vacuum state, then the output variances of the in-phase and out-of-phase quadratures are $(\mu_n + \nu_n)^2/2$ and $(\mu_n - \nu_n)^2/2$, respectively. In the Schrödinger picture (SP), the two-Schmidt-mode output state

$$|\psi_n\rangle = \sum_k (\nu_n/\mu_n)^k |k,k\rangle/\mu_n, \quad (9)$$

where $|k,k\rangle$ denotes a substate with k signal photons and k idler photons [42]. For such a state, which is pure and entangled, each photon-number mean is ν_n^2. If one ignores the idler information (by tracing out the idler degrees or freedom), one obtains a thermal signal state, which is mixed, with number mean ν_n^2. The complete state vector is the product of the two-mode state vectors. Thus, the general properties of nondegenerate FWM are known, in both the HP and SP, for arbitrary pump powers. The challenge is to determine the Schmidt coefficients and functions efficiently, and use this knowledge to optimize the designs of experiments.

Optics EXPRESS

3. Low-gain regime

Before considering the high-gain regime in detail, it is instructive to consider the low-gain regime, in which only photon pairs are produced with significant probabilities. By using the time-domain perturbation method [50, 51], which is based on the approximation that the idler response to a signal impulse is too weak to affect the signal, one obtains the HP Green functions [44]

$$\mu_{ss}(t,t') = \delta(t-t'-\beta_s l), \quad \nu_{rs}(t,t') = i\gamma_{pq}(t_c,z_c)/\beta_{rs}, \tag{10}$$

where l is the medium length, $\beta_{rs} = \beta_r - \beta_s > 0$ is the relative slowness and the signal–idler collision coordinates

$$t_c = [\beta_r t' - \beta_s(t-\beta_r l)]/\beta_{rs}, \quad z_c = [t'-(t-\beta_r l)]/\beta_{rs}. \tag{11}$$

The auxiliary condition $t'+\beta_s l < t < t'+\beta_r l$ ensures that the collision occurs within the medium. One can enforce this condition by mutiplying the cross-function ν_{rs} by $H(t-t'-\beta_s t)H(t'+\beta_r l-t)$, where $H(s)$ is a Heaviside step function. Formulas (10) are valid for arbitrary pump shapes and slownesses.

By combining Eq. (6) with the first of Eqs. (10), one obtains the reciprocity relation

$$\nu_{rs}(t_r, t_s-\beta_s l) = \nu_{sr}(t_r-\beta_r l, t_s). \tag{12}$$

Apart from time shifts, the effect of a signal impulse on the idler equals the effect of an idler impulse on the signal. By combining Eqs. (7) and (12), one finds that $v_{rn}(t) = u_{rn}(t-\beta_r l)$ and $v_{sn}(t) = u_{sn}(t-\beta_s l)$. Although the Schmidt functions are determined by the interaction of the pumps and sidebands throughout the whole medium, the output signal (idler) functions are just time-shifted versions of the input signal (idler) functions. There is no particular relation between the signal and idler functions. The argument of the shape function A_p is

$$t_c - \beta_p z_c = [\beta_{rp}t' - \beta_{sp}(t-\beta_r l)]/\beta_{rs} \tag{13}$$

and the argument of A_q is similar ($p \to q$). In general, the pump function γ_{pq} is a nonseparable function of the input and output times, so many Schmidt coefficients are nonzero and the Schmidt functions depend on both pump shapes. However, if the pumps and sidebands copropagate in a long medium ($\beta_p = \beta_r$ and $\beta_q = \beta_s$), the arguments of the shape functions reduce to $t-\beta_r l$ and t', and the auxiliary conditions can be ignored. In this case, the pump function is separable and there is only one nonzero Schmidt coefficient ($\nu_1 = \gamma/\beta_{rs} = \bar{\gamma}$), so a heralded signal would have a pure state [43, 44]. The idler Schmidt function is the shape function of pump p and the signal Schmidt function is the shape function of pump q. (The signal and idler functions also include the phase factors $e^{i\phi_r}$ and $e^{i\phi_s}$, respectively, where $\phi_r + \phi_s = \pi/2$. Henceforth, we will ignore these factors.) These shape functions can be chosen arbitrarily and independently, as required for temporal-mode multiplexing [52]. Similar results were obtained recently for photon frequency conversion by scalar nondegenerate FWM [50, 51].

In the SP, the two-photon state vector

$$|\psi_1\rangle = \int\int dt_r\, dt_s\, f(t_r,t_s) a_r^\dagger(t_r) a_s^\dagger(t_s)|\text{vac}\rangle, \tag{14}$$

where the two-photon amplitude (TPA)

$$f(t_r,t_s) = \int dt'\, \mu_{ss}(t_s,t')\nu_{rs}(t_r,t') = \int dt'\, \mu_{rr}(t_r,t')\nu_{sr}(t_s,t') \tag{15}$$

is related to the HP Green functions [44]. Integrating the product of $\mu_{jj}(t_j,t')$ and $\nu_{ij}(t_i,t')$ replaces the input Schmidt function $u_j(t')$ with the output function $v_j(t_j) = u_j(t_j-\beta_j l)$. Hence, the TPA has the Schmidt decomposition

$$f(t_r,t_s) = \textstyle\sum_n \nu_n v_{rn}(t_r) v_{sn}(t_s), \tag{16}$$

Optics EXPRESS

which involves only the output functions (as it must do). In general, the output is the entangled state $\sum_n \nu_n |\phi_{rn}\rangle|\phi_{sn}\rangle$, where $|\phi_{rn}\rangle = \int dt_r \nu_{rn}(t_r) a_r^\dagger(t_r)|\text{vac}\rangle$, but in the aforementioned special case (copropagating pumps and sidebands), it reduces to the product state $\nu_1|\phi_{r1}\rangle|\phi_{s1}\rangle$. Once again, notice that the signal and idler Schmidt (basis) functions can be chosen arbitrarily in this case.

To illustrate the low-gain results, it is convenient to choose the pump shapes from the Hermite–Gauss (HG) functions

$$\text{HG}_n(s) = H_n(s/\tau)\exp(-s^2/2\tau^2)/\pi^{1/4}(2^n n!\tau)^{1/2}, \tag{17}$$

where $H_n(s)$ is a Hermite polynomial of order n and τ is a duration (temporal width). These functions comprise a potential basis for temporal-mode multiplexing. For example, consider photon generation driven by pumps whose (common) shape function is a Gauss (zeroth-order HG) function (HG_0). In Fig. 1, the cross-function ν_{rs} is plotted as a function of the input and output times for two cases. In the first case, the pumps and sidebands copropagate ($\beta_r = \beta_p$ and $\beta_s = \beta_q$), but the medium is not long enough for a complete pump–pump collision. In the second case, the medium is long enough for a complete collision, but the pumps and sidebands do not copropagate ($\beta_r \neq \beta_p$ and $\beta_s \neq \beta_q$). Both cases exhibit strong correlations between the input and output times.

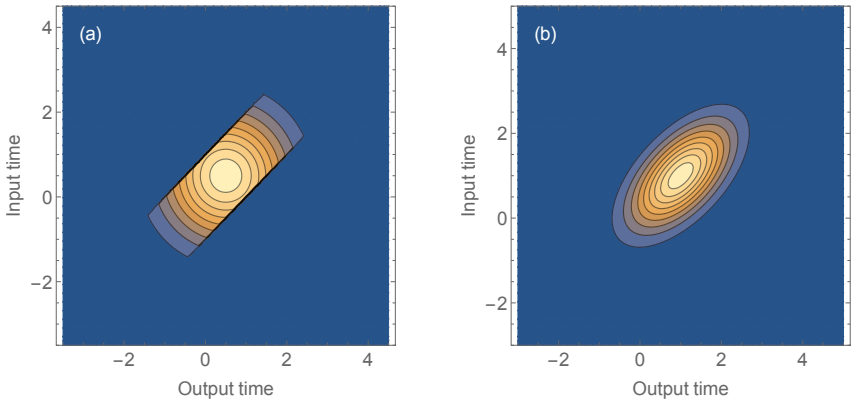

Fig. 1. Contour plot of the Green function ν_{rs} for two cases in which the pump shapes are Gauss (HG_0) functions. (a) $\beta_p l/\tau = \beta_r l/\tau = 1$ and $\beta_q l/\tau = \beta_s l/\tau = -1$. (b) $\beta_p l/\tau = 4 = -\beta_q l/\tau$ and $\beta_r l/\tau = 2 = -\beta_s l/\tau$. Lighter shading represents higher values, whereas darker shading represents lower values. Time is measured in units of τ. The input and output times are correlated.

In Fig. 2, the normalized Schmidt coefficient $\nu/\bar{\gamma}$ is plotted as a function of the mode number n. In both of the aforementioned cases, several Schmidt coefficients are nonzero, so heralded signals have mixed states. The Schmidt functions (not shown) have widths that differ from the (common) pump width τ. Some results for copropagating pumps and sidebands, which confirm the prediction that heralded signals have pure states, were illustrated in [44]. More such results will be illustrated shortly, as low-gain limits of arbitrary-gain results [Figs. 5(a), 7(a)–9(a) and (10)].

Optics EXPRESS

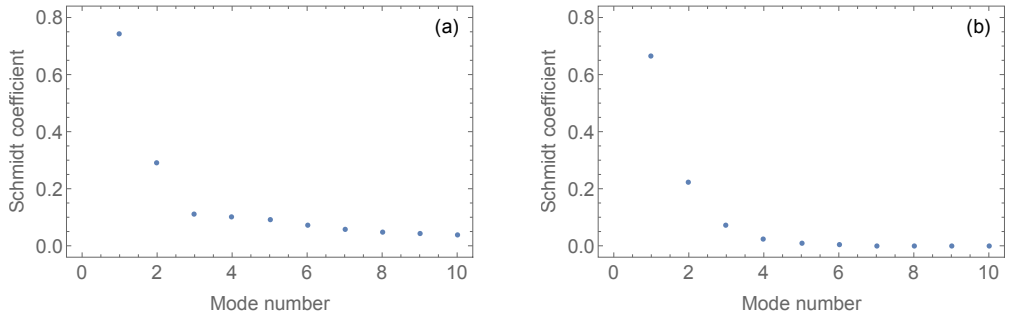

Fig. 2. The normalized Schmidt coefficient is plotted as a function of mode number for two HG_0 pumps. (a) $\beta_p l/\tau = \beta_r l/\tau = 1$ and $\beta_q l/\tau = \beta_s l/\tau = -1$. (b) $\beta_p l/\tau = 4 = -\beta_q l/\tau$ and $\beta_r l/\tau = 2 = -\beta_s l/\tau$. Several coefficients are nonzero.

4. Arbitrary-gain regime

Armed with the insight provided by the low-gain results, it is now appropriate to consider the interaction of copropagating pumps and sidebands ($\beta_p = \beta_r$ and $\beta_q = \beta_s$) in the arbitrary-gain regime. Simultaneous slowness and wavenumber matching is exhibited by vector FWM in a SBM, which is illustrated in Fig. 3. The pump frequencies can be varied independently.

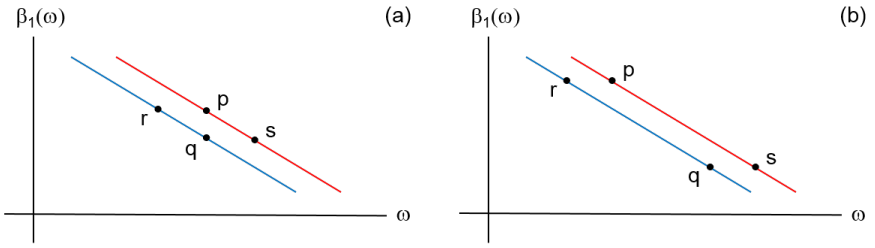

Fig. 3. Frequency diagrams for vector four-wave mixing in a strongly-birefringent medium [44]. Points on the blue (red) curves denote waves that are aligned with the fast (slow) axes of the medium. The wavenumbers and slownesses (β_1) are matched simultaneously for pump frequencies that are (a) degenerate and (b) nondegenerate. Notice that the copropagating waves have different polarizations. The pump and sideband frequencies can be interchanged ($p \leftrightarrow r$ and $q \leftrightarrow s$). The displayed diagrams pertain to the anomalous dispersion regime and similar diagrams pertain to the normal dispersion regime.

The CMEs are partial differential equations with space- and time-varying coefficients. Nonetheless, by using standard mathematical methods [53, 54], which are sketched in the appendix, one can solve them analytically for arbitrary pump powers and shapes. The final results are

$$\begin{aligned} \mu_{ss}(t,t') &= \delta(t-t'-\beta_s l) + \bar{\gamma} A_q(t-\beta_s l)(\xi/\eta)^{1/2} I_1[2\bar{\gamma}(\xi\eta)^{1/2}] A_q(t') \\ &\quad \times H(t-t'-\beta_s l) H(t'+\beta_r l - t), \end{aligned} \tag{18}$$

$$\nu_{rs}(t,t') = i\bar{\gamma} A_p(t-\beta_r l) I_0[2\bar{\gamma}(\xi\eta)^{1/2}] A_q(t') H(t-t'-\beta_s l) H(t'+\beta_r l - t), \tag{19}$$

where $I_m(s)$ is a modified Bessel function of order m and the interaction distances

$$\xi(t,t') = \int_{t-\beta_r l}^{t'} ds |A_p(s)|^2, \quad \eta(t,t') = \int_{t'}^{t-\beta_s l} ds |A_q(s)|^2. \tag{20}$$

The step functions enforce causality: For each input point $(t', 0)$ they define the region of influence and for each output point (t, l) they define the domain of dependence. The interaction distances

Optics EXPRESS

are proportional to the pump energies contained within the interaction region, which is the intersection of the aforementioned domain and region. The formulas for the other two Green functions are similar ($r \leftrightarrow s$ and $\xi \leftrightarrow \eta$).

Formulas (18)–(20) are complicated. Nonetheless, it is posssible to make some general observations. According to the Schmidt formalism, which was described above, the Schmidt coefficients and the four sets of Schmidt functions are specified completely by the cross-functions ν_{rs} and ν_{sr} (or the self-functions μ_{rr} and μ_{ss}). Consider the former pair of Green functions. The input-signal Schmidt functions are eigenfunctions of the signal kernel

$$k_s(t_s, t_s') = \int dt_r \nu_{rs}^*(t_r, t_s)\nu_{rs}(t_r, t_s'), \tag{21}$$

whereas the output-idler Schmidt functions are eigenfunctions of the idler kernel

$$k_r(t_r, t_r') = \int dt_s \nu_{rs}(t_r, t_s)\nu_{rs}^*(t_r', t_s). \tag{22}$$

It is easy to show that if $u_s(t_s)$ is an eigenfunction of the signal kernel, then $v_r(t_r) = \int dt_s \nu_{rs}(t_r, t_s)u_s(t_s)$ is an eigenfunction of the idler kernel and is associated with the same eigenvalue. Conversely, if $v_r(t_r)$ is an eigenfunction of the idler kernel, then $u_s(t_s) = \int dt_r \nu_{rs}^*(t_r, t_s)v_r(t_r)$ is an eigenfunction of the idler kernel. Hence, the signal and idler kernels have the same eigenvalues, which are non-negative. The (common) Schmidt coefficients are the square roots of these eigenvalues. Similar statements can be made about the input-idler and output-signal Schmidt functions. In general, the Green functions (interaction distances and step functions) are nonseparable functions of the input and output times, so one should expect several Schmidt coefficients to be nonzero and the Schmidt functions to depend on both pump shapes.

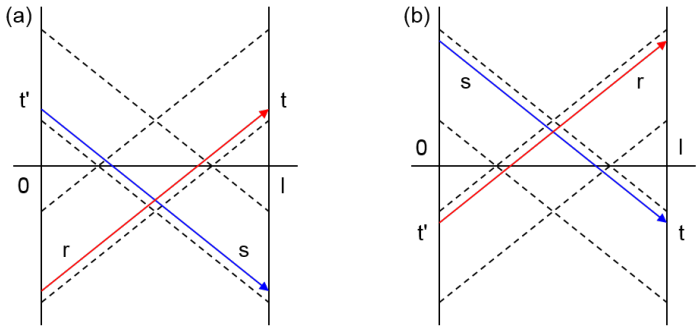

Fig. 4. Characteristic diagram for (a) idler generation and (b) signal generation. The horizontal axis is distance and the vertical axis is time. The interaction is limited to the region in which the pumps collide, which is the interior of the dashed diamond. The blue and red rays (arrows) represent parts of the signal and idler that interact strongly.

For a complete collision, which is illustrated in Fig. 4, both step functions are equal to 1. For the cross-function ν_{rs}, in the formula for ξ one can replace the upper limit t' by ∞ and in the formula for η one can replace the upper limit $t - \beta_s l$ by ∞. With these replacements, the input signal function is determined solely by $A_q(t')$ and the output idler function is determined solely by $A_p(t - \beta_r l)$. The Green function is proportional to $\bar{\gamma} I_0\{2\bar{\gamma}[\xi(t - \beta_r l)\eta(t')]^{1/2}\}$. This reduced function is separable in the low-gain regime and asymptotically separable in the high-gain regime (as explained in the appendix), so the Schmidt decomposition of ν_{rs} involves only a single nonzero Schmidt coefficient and a single pair of Schmidt functions in both regimes. For ν_{sr}, in the formulas for ξ and η one can replace the lower limits $t - \beta_r l$ and t' by $-\infty$. With these replacements, the input idler function is determined solely by $A_p(t')$ and the output signal function is determined solely by $A_q(t - \beta_s l)$. The reduced function $\bar{\gamma} I_0\{2\bar{\gamma}[\xi(t')\eta(t - \beta_s l)]^{1/2}\}$

Optics EXPRESS

is also approximately separable in the low- and high-gain regimes, so the decomposition of ν_{sr} also involves only a single nonzero coefficient and a single pair of functions in both regimes. Notice that A_p and A_q are always paired with ξ and η, respectively. The results that follow all pertain to complete collisions.

4.1. Schmidt coefficients

In Fig. 5, the first (largest) Schmidt coefficient ν_1 is plotted as a function of the gain parameter $\bar{\gamma}$, for two different combinations of HG pump shapes. In the low-gain regime ($\bar{\gamma} \leq 0.5$), the coefficient is a linear function of gain and does not depend on the pump shapes, as predicted by Eq. (10) and the corresponding limit of Eq. (19). In the high-gain regime ($\bar{\gamma} \geq 2$), the coefficient is a nearly-exponential function of gain and still does not depend on the pump shapes! The formula stated in the caption was derived by using the high-gain limit of the modified Bessel function. This derivation and an explanation of why the coefficient does not depend on the pump shapes are provided in the appendix. In both regimes, the associated Schmidt state contains $2\nu_1^2$ photons on average.

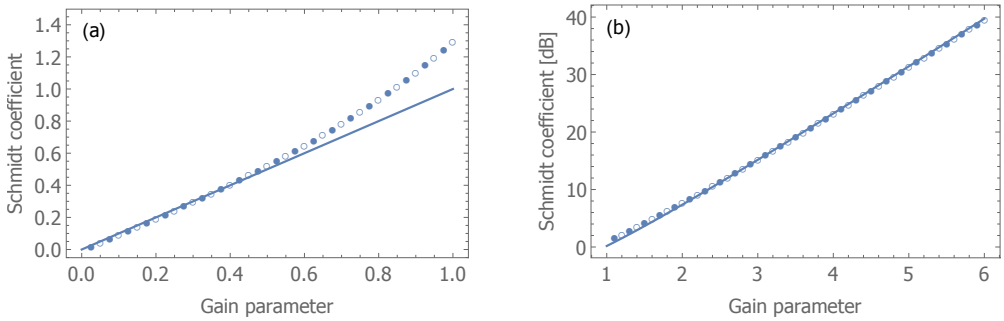

Fig. 5. The first Schmidt coefficient is plotted as a function of the gain parameter $\bar{\gamma}$. In (a) the solid line is $\bar{\gamma}$ and the vertical scale is linear, whereas in (b) the solid curve is $\exp(2\bar{\gamma})/(16\pi\bar{\gamma})^{1/2}$ and the scale is logarithmic. Filled circles denote results for two HG_0 pumps, whereas empty circles denote results for one HG_0 and one HG_1 pump. The Schmidt coefficients do not depend on the pump shapes.

In Fig. 6, the ratio of the second Schmidt coefficient to the first (ν_2/ν_1) is plotted as a function of gain, for two different combinations of pump shapes. For both combinations, this ratio starts at zero, as predicted by perturbation theory, increases to its peak value of 0.1, then decreases monotonically. The relative probability of the second mode pair, which is the square of this ratio, does not exceed 1%. Thus, for all practical purposes, vector FWM produces a single pair of Schmidt modes for arbitrary pump powers and shapes. Similar single-mode behavior is exhibited by transient spontaneous Raman scattering (SRS) [55]. This behavior contrasts with the behavior of frequency conversion, in which the number of active Schmidt modes is an increasing function of the pump powers [50, 51].

Based on the preceding results for vector FWM and SRS, one might suspect that every unstable two-sideband process exhibits single-mode operation. There is certainly a tendancy for unstable processes to be dominated by the modes that grow most rapidly in space and time [56–58]. However, we made a preliminary anaysis of another (common) process, in which the signal copropagates with a single pump (or two copropagating pumps), but the idler does not. In this process the pump is always present (or the pumps always overlap) and several temporal modes, with comparable Schmidt coefficients, are produced.

Optics EXPRESS

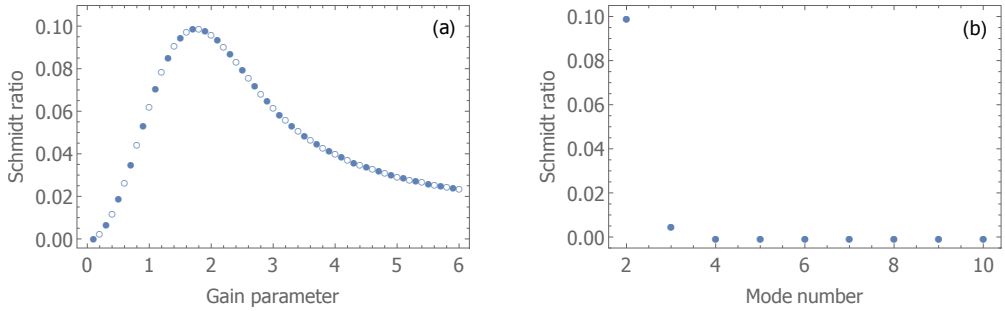

Fig. 6. (a) The ratio of the second Schmidt coefficient to the first is plotted as a function of the gain parameter $\bar{\gamma}$. Filled circles denote results for two HG_0 pumps, whereas empty circles denote results for one HG_0 and one HG_1 pump. The relative probability of the second mode, which is the square of the Schmidt ratio, never exceeds 1%. (b) The Schmidt ratio is plotted as a function of mode number for the worst case, in which $\bar{\gamma} = 1.76$. The HG_0-HG_0 and HG_0-HG_1 results are indistinguishable.

4.2. *Schmidt functions*

The cross-function ν_{rs} [Eq. (19)] is illustrated in Fig. 7, for pump shapes that are Gauss functions, and small and large gain values. In this figure and the ones that follow, time is measured in units of the pump width τ [Eq. (17)]. In the low-gain regime, the cross-function is the symmetic product of two Gauss functions, as predicted by perturbation theory [Eq. (10)]. In the high-gain regime, it is compact, and skewed toward earlier input and output times [Eq. (19)].

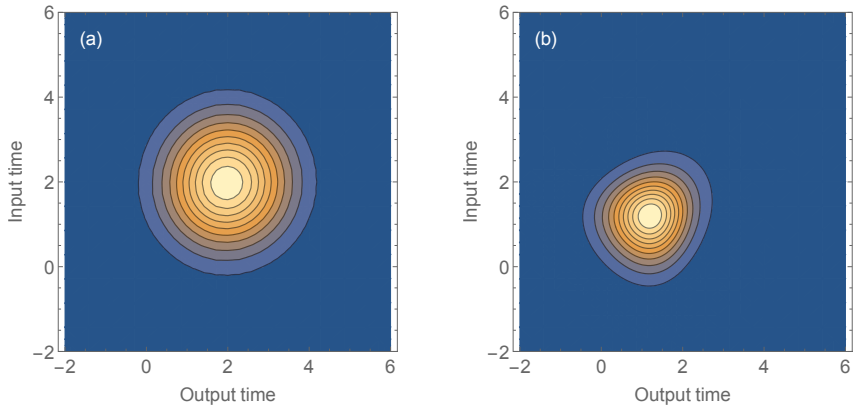

Fig. 7. Contour plots of the Green function ν_{rs} for the gain parameters (a) $\bar{\gamma} = 0.3$ and (b) $\bar{\gamma} = 3.0$. Both pump shapes are Gauss (HG_0) functions. Lighter shading represents higher values, whereas darker shading represents lower values. High gain localizes the Green function near early input and output times.

Because the pump shapes are identical, so also are the signal and idler Schmidt functions. The (common) Schmidt function is illustrated in Fig. 8. In the low-gain regime, the Schmidt function is approximately Gaussian. In the high-gain regime it is skewed toward earlier input and output times, like the Green function with which it is associated. This phenomenon can be explained. Idler generation is illustrated in Fig. 4(a). In physical terms, as the input signal ray (shown) propagates to the lower right, it seeds idler rays that propagate to the upper right (not

Optics EXPRESS

shown). In turn, these idler rays seed signal rays (not shown) that propagate to the lower left and interact with the idler rays. Thus, the sidebands grow in the part of the collision region that is above and to the right of the input signal ray. Earlier idler rays (one of which is shown) represent parts of the idler that interact with stronger parts of the signal and grow more. In mathematical terms, the argument of the modified Bessel function is proportional to the square root of the area of the growth region, which is larger for signal and idler rays that correspond to earlier input and output times. Similar skewing is exhibited by transient SRS [49]. This phenomenon is characteristic of instabilities, in which the output is dominated by the source points (times) associated with higher gains. For signal generation [Fig. 4(b)], the input idler and output signal functions (not shown) are advanced relative to the previous ones, and are skewed toward later times, for a reason similar to that stated above.

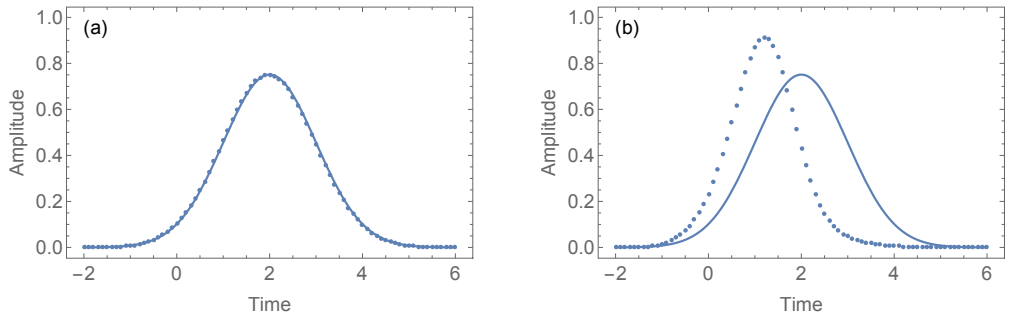

Fig. 8. The (common) signal and idler Schmidt function (dots) is plotted as a function of time for the gain parameters (a) $\bar{\gamma} = 0.3$ and (b) $\bar{\gamma} = 3.0$. Both pump shapes (solid curves) are Gauss (HG_0) functions. In the low-gain regime the Schmidt function is approximately Gaussian, whereas in the high-gain regime it is a distorted Gaussian.

Similar behavior occurs for other pump shapes. The cross-function ν_{rs} is illustrated in Fig. 9, for pumps that are zeroth- and first-order HG functions, and small and large gain values. The associated input and output Schmidt functions are illustrated in Figs. 10 and 11, respectively.

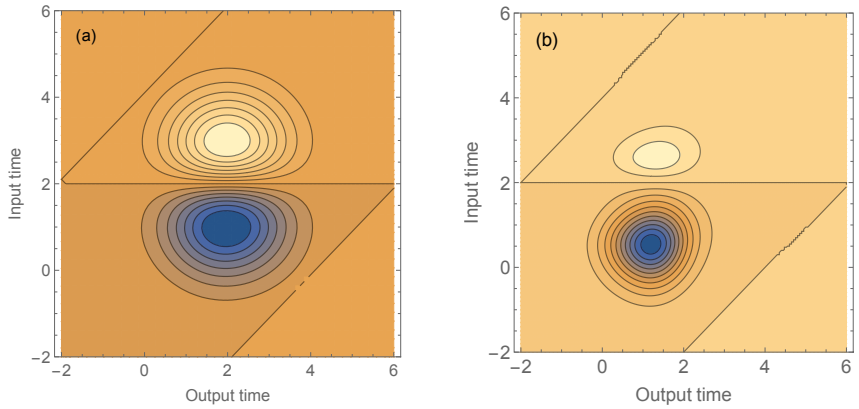

Fig. 9. Contour plots of the Green function ν_{rs} for the gain parameters (a) $\bar{\gamma} = 0.3$ and (b) $\bar{\gamma} = 3.0$. The pump shapes are HG_0 and HG_1 functions. Lighter shading represents higher values, whereas darker shading represents lower values. High gain localizes the Green function near early input and output times.

Optics EXPRESS

In the low-gain regime, the Green and Schmidt functions are approximately HG functions, as predicted by perturbation theory. In the high-gain regime, all three functions are skewed toward earlier input and output times.

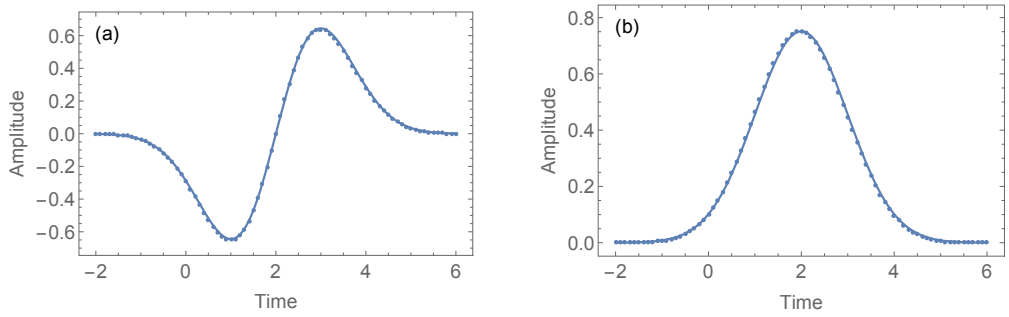

Fig. 10. The input signal (a) and output idler (b) Schmidt functions (dots) are plotted as functions of time for the gain parameter $\bar{\gamma} = 0.3$. The pump shapes (solid curves) are HG_0 and HG_1 functions. In the low-gain regime both Schmidt functions are approximately HG functions.

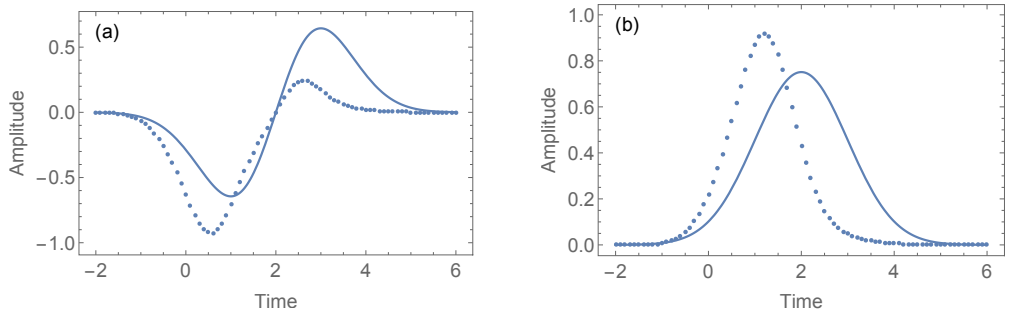

Fig. 11. The input signal (a) and output idler (b) Schmidt functions (dots) are plotted as functions of time for the gain parameter $\bar{\gamma} = 3.0$. The pump shapes (solid curves) are HG_0 and HG_1 functions. In the high-gain regime both Schmidt functions are distorted HG functions.

5. Nonlinear phase modulation

Equations (1) and (2) do not include the effects of NPM, which can chirp the pumps, signal and idler, and dephase the interaction [44, 59–61]. To obtain a Green matrix, we solved the CMEs for FWM and NPM numerically, for many HG_n input signals, and decomposed the output idlers in terms of the same basis functions. Subsequently, we decomposed this matrix numerically [62].

Some results of such simulations are shown in Figs. 12 and 13. In all the simulations, the medium length $l = 80$ m, the relative slowness $\beta_1 = \beta_{rs} = 0.5$ ps/m, the second-order dispersion coefficient $\beta_2 = 15$ ps^2/Km and the Kerr nonlinearity coefficient $\gamma_K = 10$/Km-W. The input pumps have Gauss (HG_0) shape functions with (common) width $\tau = 5$ ps. The fast pump (q) is delayed by 10 ps at the input and the slow pump (p) is advanced by 10 ps, so the pumps overlap completely in the middle of the medium. These parameters are typical of silica fibers. Experiments are also feasible in silicon chips, in which higher birefringence and nonlinearity

Optics EXPRESS

compensate for shorter length [62]. The nonlinear effect of each pump on itself (self-phase modulation) is a chirp, whereas the effect of each pump on the other (cross-phase modulation) is a wavenumber shift. We chose to prechirp the input pumps so that they are approximately unchirped in the middle of the medium, where their interaction with the signal and idler is strongest.

In Fig. 12, the ratio of the second Schmidt coefficient to the first (ν_2/ν_1) is plotted as a function of the gain parameter $\bar{\gamma}$. (For the chosen parameters, $\bar{\gamma} = 1$ corresponds to a peak pump power of 5.6 W.) The numerical Schmidt ratios are higher than the semi-analytical ratios. However, the numerical and semi-analytical curves are qualitatively similar and for no value of the gain parameter (in the chosen range) does the numerical result exceed the semi-analytical result by more than a factor of 2. In particular, the maximal value of the numerical ratio is 0.13, which corresponds to a relative Schmidt-mode probability of only 1.7%. For the parameters chosen, NPM does not increase the Schmidt ratio significantly, because most of the induced phase shifts are chirps (separable functions of t and t'). We also simulated photon generation by shorter (1-ps) pulses, for which the effects of dispersion are stronger [62]. In these simulations, the numerical and semi-analytical results were also comparable for small and medium values of the gain parameter, but the numerical results started to diverge from the semi-analytical ones at $\bar{\gamma} = 4$. This value corresponds to a gain of more than 40 dB (expected photon number larger than 10^4), so NPM does not prevent single-mode operation for a useful range of pump powers.

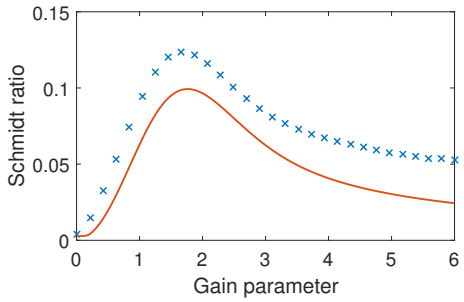

Fig. 12. The ratio of the second Schmidt coefficient to the first is plotted as a function of the gain parameter $\bar{\gamma}$ for two Gauss (HG_0) pumps. The solid curve denotes semi-analytical results that omit nonlinear phase modulation, whereas crosses denote numerical results that include nonlinear phase modulation. The results are qualitatively similar and quantitatively comparable.

In Fig. 13, the amplitudes and phases of the input-signal and output-idler Schmidt functions are plotted as functions of time for the gain parameter $\bar{\gamma} = 1.55$, which corresponds to expected signal and idler photon numbers of 10. The amplitude profiles of the signal and idler are similar, but not identical. Both pulses are skewed toward early times, as predicted by theory, but the idler is skewed slightly more than the signal. The signal and idler are chirped in opposite ways and the chirps are centered on the peaks of the copropagating pumps. The signal phase has a net negative slope, which corresponds to a positive frequency shift, whereas the idler phase has a net positive slope, which corresponds to a negative frequency shift. These shifts are measured relative to the frequencies that correspond to wavenumber matching at zero pump power. The signal and idler frequencies are shifted toward the pump frequencies, as required to achieve wavenumber matching for nonzero power [44, 48]. For reference, the input idler and output signal functions (not shown) are time-reversed images of the displayed input and output functions.

A comprehensive set of simulation results will be described in a future publication. However, the representative results described herein show that NPM is not a fundamental obstacle to the generation of signal and idler photons in single pairs of Schmidt modes. If necessary, the signal and idler chirps can be removed by propagation in a dispersive medium.

Optics EXPRESS

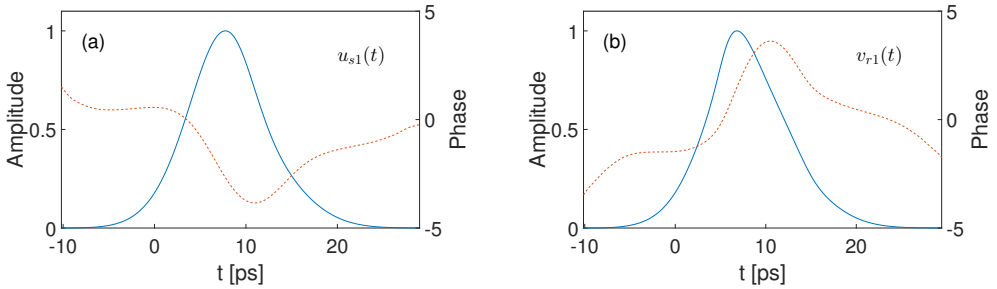

Fig. 13. The amplitudes (blue curves) and phases (red curves) of the input signal (a) and output idler (b) Schmidt functions are plotted as functions of time for the gain parameter $\bar{\gamma} = 1.55$. Both pump shapes are Gauss (HG_0) functions. Nonlinear phase modulation imposes opposite chirps and frequency shifts on the signal and idler. The chirps are extremal near the peaks of the copropagating pumps, relative to which the signal and idler are skewed toward early times.

6. Summary

In summary, photon generation by vector four-wave mixing (FWM) in a strongly birefringent medium was studied in detail. In this process, the signal copropagates with one pump, the idler copropagates with the other, and the medium is long enough for a complete pump–pump collision. This configuration enables the generation of signal and idler photons in a single pair of temporal (Schmidt) modes. The shapes of the signal and idler wavepackets (Schmidt functions) can be specified arbitrarily and indepedently by controlling the pump shapes, as required for temporal-mode multiplexing [52]. For low pump powers, the Schmidt coefficients (square roots of the photon probabilities) are less than 1 and increase linearly with the power parameter (square root of the product of the pump energies). The Schmidt functions match the pump shapes closely and the output functions (which describe the detection probabilities of emitted photons) are just time-shifted versions of the input functions (which describe the seeding probabilities of virtual input photons). For high pump powers, the Schmidt coefficients are greater than 1 and increase nearly exponentially with power. The Schmidt functions are distorted versions of the pump shapes. The input signal and output idler functions are skewed toward earlier times, whereas the input idler and output signal functions are skewed toward later times. Such skewing maximizes the gain experienced by the signal and idler during their spatial–temporal interaction. As the pump powers increase, the relative probability of the second pair of Schmidt modes to the first pair increases from 0 to 1%, then decreases. Nonlinear phase modulation does not increase the modal diversity significantly for gains less than 40 dB. Thus, for all practical purposes, vector FWM produces a single pair of temporal modes for a wide range of pump powers and arbitrary pump shapes. We believe that these properties and frequency tunability [44] make vector FWM a versatile tool for quantum information science.

Appendix: Derivation of the Green functions

In the undepleted-pump regime, the CMEs for the signal and idler amplitudes are

$$(\partial_z + \beta_r \partial_t) A_r = i\gamma_{pq} A_s^* + \sigma_r \delta(z)\delta(t), \quad (\partial_z + \beta_s \partial_t) A_s = i\gamma_{pq} A_r^* + \sigma_s \delta(z)\delta(t), \tag{23}$$

where the pump function $\gamma_{pq} = \gamma A_p(t - \beta_p z) A_q(t - \beta_q z)$ and $\sigma_j = 0$ or 1, depending on which mode is seeded by an impulse. The physical CMEs are difficult to solve, because they are partial differential equations with coefficients that depend on distance and time. However, there is at least one important case in which they can be solved.

Optics EXPRESS

For vector FWM in a SBM [45–48], there exist pump, signal and idler frequencies for which $\beta_p = \beta_r$ and $\beta_q = \beta_s$. (Similar conditions facilitated the analysis of frequency conversion in an isotropic fiber [50, 51].) Without loss of generality, suppose that $\beta_r > \beta_s$, and define the characteristic variables $x = \beta_r z - t$ and $y = t - \beta_s z$. Then the characteristic CMEs are

$$\partial_y A_r = i\bar{\gamma} A_p(-x) A_q(y) A_s^* + \sigma_r \delta(x)\delta(y), \quad \partial_x A_s = i\bar{\gamma} A_p(-x) A_q(y) A_r^* + \sigma_s \delta(x)\delta(y), \tag{24}$$

where $\bar{\gamma} = \gamma/\beta_{rs}$, $\beta_{rs} = \beta_r - \beta_s$ and $\delta(z)\delta(t) = \beta_{rs}\delta(x)\delta(y)$.

Now let $A_r/A_p \to A_r$ and $A_s/A_q \to A_s$, and define the interaction distances $\xi = \int_{-x}^{0} |A_p(x')|^2 dx'$ and $\eta = \int_0^y |A_q(y')|^2 dy'$. (The normalization factors A_p and A_q are evaluated at $-x$ and y, respectively.) Then the canonical CMEs are

$$\partial_\eta A_r = i\bar{\gamma} A_s^* + \sigma_r A_p^* \delta(\xi)\delta(\eta), \quad \partial_\xi A_s = i\bar{\gamma} A_r^* + \sigma_s A_q^* \delta(\xi)\delta(\eta), \tag{25}$$

where $\delta(x) = |A_p|^2\delta(\xi)$ and $\delta(y) = |A_q|^2\delta(\eta)$. (The source strengths $|A_p|^2$ and $|A_q|^2$ are evaluated at 0.) Notice that Eqs. (25) do not depend explicitly on the pump shapes. They are mathematically equivalent to the CMEs for SBS and SRS, which involve only a single pump and its associated interaction distance. Their solutions can be written in the IO forms of Eqs. (4). The Green functions associated with a signal source of unit strength at the origin are [53, 54]

$$G_{rs}(\xi,\eta) = i\bar{\gamma} I_0[2\bar{\gamma}(\xi\eta)^{1/2}] H(\xi)H(\eta), \tag{26}$$

$$G_{ss}(\xi,\eta) = \bar{\gamma}(\xi/\eta)^{1/2} I_1[2\bar{\gamma}(\xi\eta)^{1/2}] H(\xi)H(\eta) + H(\xi)\delta(\eta), \tag{27}$$

where $I_m(s)$ is a modified Bessel function of order m and $H(s)$ is a Heaviside step function. The Green functions associated with an idler source are similar ($r \leftrightarrow s$ and $\xi \leftrightarrow \eta$). In particular, the cross functions satisfy the reciprocity relation $G_{rs}(\xi,\eta) = G_{sr}(\xi,\eta)$. To account for sources at other locations, one makes the replacements $\xi \to \xi - \xi'$ and $\eta \to \eta - \eta'$.

For any parametric process, the Green functions all have Schmidt decompositions, which involve Schmidt coefficients and functions. Because these decompositions are related, it is sufficient to decompose the cross-functions G_{rs} (which involves the input signal and output idler functions) and G_{sr} (which involves the input idler and output signal functions). First, consider G_{rs}. For a complete collision, the effective (signal) input point is $(0, \eta')$ and the effective (idler) output point is $(\xi, 1)$. (For incomplete collisions, the formulas for the input and output points can be complicated.) In the low-gain regime ($\bar{\gamma} \ll 1$), $G_{rs} \approx \bar{\gamma}$. One can rewrite this result in the Schmidt form $G_{rs}(\xi,\eta') \approx v(\xi)vu(\eta')$, where $v = \bar{\gamma}$ and $u(s) = v(s) = H(s)H(1-s)$. In the high-gain regime ($\bar{\gamma} \gg 1$), one can use the asymptotic formula $I_0(s) \sim \exp(s)/(2\pi s)^{1/2}$ to write

$$G_{rs}(\xi,\eta') \sim \frac{\bar{\gamma}\exp[2\bar{\gamma}\xi^{1/2}(1-\eta')^{1/2}]}{(4\pi\bar{\gamma})^{1/2}} \sim \frac{\bar{\gamma}\exp[2\bar{\gamma} - \bar{\gamma}(1-\xi) - \bar{\gamma}\eta')]}{(4\pi\bar{\gamma})^{1/2}}. \tag{28}$$

Hence, $G_{rs}(\xi,\eta') \sim v(1-\xi)vu(\eta')$, where $v = \exp(2\bar{\gamma})/(16\pi\bar{\gamma})^{1/2}$ and $u(s) = v(s) = (2\bar{\gamma})^{1/2}$ $\exp(-\bar{\gamma}s)$. The signal function is skewed toward smaller values of η' and the idler function is skewed toward larger values of ξ. In both the low- and high-gain regimes, the decomposition involves only a single pair of Schmidt modes. Second, consider G_{sr}, for which the effective input (idler) point is $(\xi', 0)$ and the effective output (signal) point is $(1, \eta)$. The decomposition of this cross-function is similar to the previous decomposition, the only differences being that the idler function is skewed toward smaller values of ξ' and the signal function is skewed toward larger values of η. Apart from reflections in characteristic coordinates, the signal and idler Schmidt functions are identical, as required by reciprocity.

To convert the canonical Green functions to physical functions, one multiplies G_{rr} and G_{sr} by $A_p^*(0)$, and G_{rs} and G_{ss} by $A_q^*(0)$. One also multiplies G_{rr} and G_{rs} by $A_p(-x)$ and G_{sr} and

Optics EXPRESS

G_{ss} by $A_q(y)$. Then one rewrites the characteristic variables in terms of the physical variables ($0 \to t'$, $-x \to t - \beta_r z$ and $y \to t - \beta_s z$.) The final results are

$$\begin{aligned} G_{rs}(t,t') &= \bar{\gamma} A_p(t-\beta_r l) I_0[2\bar{\gamma}(\xi\eta)^{1/2}] A_q(t') \\ &\quad \times H(t-t'-\beta_s l) H(t'+\beta_r l - t), \end{aligned} \tag{29}$$

$$\begin{aligned} G_{ss}(t,t') &= \delta(t-t'-\beta_s l) + \bar{\gamma} A_q(t-\beta_s l)(\xi/\eta)^{1/2} I_1[2\bar{\gamma}(\xi\eta)^{1/2}] A_q(t') \\ &\quad \times H(t-t'-\beta_s l) H(t'+\beta_r l - t), \end{aligned} \tag{30}$$

where the interaction distances

$$\xi(t,t') = \int_{t-\beta_r l}^{t'} ds |A_p(s)|^2, \quad \eta(t,t') = \int_{t'}^{t-\beta_s l} ds |A_q(s)|^2. \tag{31}$$

The physical Schmidt coefficients equal the canonical coefficients, and the physical Schmidt functions are the canonical functions multiplied by the appropriate pump-shape functions. (The canonical functions skew the physical functions.) For a system with a Hamiltonian that is quadratic in the mode amplitudes (operators), the Heisenberg equations for the mode operators are identical to the Hamilton equations for the mode amplitudes. Hence, the quantum Green functions are identical to the classical functions derived in this appendix.

Funding

Danish National Research Foundation (DNRF-123); Danish Council for Independent Research (DFF-4184-00433); DFF Sapere Aude (NANO-SPECs); Huawei Technologies; National Science Foundation (NSF-1521466).

Acknowledgments

This work was initiated during a visit by CM to the Technical University of Denmark, which was supported by the Silicon Photonics for Optical Communications Centre. CM would like to thank Leif Oxenløwe for his hospitality.